Carbon dot based hyperbranched epoxy nanocomposites

Highlight

This chapter deals with the fabrication of carbon dot based hyperbranched epoxy nanocomposites to achieve interesting optical properties along with tremendous improvement in overall performance for potential utilization in different fields including optoelectronic. The chapter is divided into three sub-chapters, where first sub-chapter describes synthesis, characterization and property evaluation of fluorescent carbon dot nanomaterial. Second sub-chapter deals with the fabrication of high performance photoluminescent transparent hyperbranched epoxy/carbon dot nanocomposite obtained by solution technique. The last sub-chapter demonstrates fabrication and characterization of a high performance, light emitting and transparent hyperbranched epoxy/carbon dot *in-situ* nanocomposite where carbon dot covalently bonded with hyperbranched epoxy. In both the cases, the resultant hyperbranched epoxy nanocomposites exhibited high performance along with interesting optical properties. The nanocomposite describes in the last sub-chapter, possesses superior properties compared to pristine hyperbranched epoxy thermoset as well as its *ex-situ* nanocomposite with carbon dot. All these nanocomposites have great potential as high performance thermosetting materials in various fields including optoelectronics.

Parts of this chapter are published in

1. B. De and N. Karak, *RSC Adv*. **3**, 8286-8290, 2013.
2. B. De, B. Voit and N. Karak, *ACS Appl. Mater. Interfaces* **5**, 10027-10034, 2013.
3. B. De, M. Kumar, B. B. Mandal and N. Karak, *RSC Adv.* 2015 (Revision submitted).

4A. Bio-precursor, *Musa acuminata* based carbon dot

4A.1. Introduction

The importance of hyperbranched epoxy nanocomposite was clearly observed from the last chapter. The formation of suitable epoxy naocomposites with different types of nanomaterials is also reported in large number of literature for the same purpose.[1-3] Recently, epoxy/quantum dot nanocomposites have captured tremendous interest to obtain high transparency and high luminescence solid films for advanced optoelectronics. Zou et al. reported a transparent and luminescent epoxy nanocomposite with CdSe quantum dots.[4] Yang et al. reported transparent and light-emitting epoxy nanocomposites containing ZnO quantum dots as encapsulating materials for solid state lighting.[5] However, in all aforementioned cases inorganic semiconductor quantum dots were mainly used and no report on performance of the resulted nanocomposites was found. Thus, the improvement in performance of luminescent materials is limited for advanced optoelectronics application. In this respect, carbon quantum dot or carbon dot is a novel class of fluorescent material and an attractive alternate to the traditional semiconductor nanocrystals due to its superior properties. These include resistance to photobleaching, chemical inertness, no optical blinking, easy functionalizability, non toxicity or biocompatibility and water solubility.[6-10] It is a young smart member of carbon nanomaterials' family, first obtained during purification of single-walled carbon nanotubes in 2004.[11] It is generally oxygenous carbon nanoparticles with size below 10 nm.[12] Carbon dot gradually becomes exciting nanomaterials because of its benign and inexpensive nature with easy availability, which resulted numerous possible applications in optoelectronics and energy sector, biomedical science, sensor and catalysis.[13] Several strategies are demonstrated for the synthesis of carbon dot with desired properties. High energy ion beam radiation and laser ablation are two common approaches for the preparation of carbon dot from cement and graphite powders.[13,14] However, to prevent the use of expensive precursors and energetic systems, different chemical methods are being adopted. Oxidation of gas soot, carbon soot or activated carbon using strong acids like nitric acid are also relatively inexpensive way to prepare carbon dot,[15,16] but the use of large amount of such strong acids is undesirable and hazardous. Again, the carbonization of glucose, sucrose, glycol, glycerol, citric acid, ascorbic acid, etc. has achieved significant attention for the production of fluorescent carbon dot as precursors, though most of these methods need multi-step operations and strong acids as well as post-treatment with surface passivating agents to improve the water solubility and luminescent properties.[17-19] Recently, serious efforts are being made to obtain self-passivated

carbon dot by one step hydrothermal carbonization with high temperature or microwave assisted hydrothermal carbonization of different carbon precursors.[20-24] However, again all these methods suffer from some drawbacks like requirement of complex and time consuming process, high temperature, harsh synthetic conditions and hence highly expensive, which limit their wide applications. Thus, the production of carbon dot from renewable bio-precursor with inexpensive and greener method is a challenging but worthy concept. Many researchers reported such types of endeavor from readily available natural bio-resources, like orange peel, pericarp, peppermint oil, cow milk, food-waste, natural proteins, etc.[24-29] However, in most of these cases the yield of carbon dot was found to be very low.

Thus, in the present sub-chapter, a facile and greener synthetic approach with high yield of carbon dot was reported by simply heating of banana juice. The formation of carbon dot and its characterization and luminescence behavior under varieties of conditions were delved into.

4A.2. Experimental

4A.2.1. Materials

Banana (*Musa acuminata*) (**Figure 4A.1**) was used as a bio-resource for the synthesis of carbon dot. It was purchased from the local market of Assam, India. Banana mainly contains water along with 20-25% carbohydrates, 1-3% ascorbic acid and trace amount of some metals. Carbohydrates and ascorbic acid are the main carbon precursors for the synthesis of carbon dot.

Figure 4A.1: Picture of banana (*Musa acuminata*), used as the bio-source

EtOH solvent was purchased from Merck, India as reported in Chapter 2.

Quinine sulfate (**Figure 4A.2**) was used as the standard for the measurement of fluorescent quantum yield of carbon dot. It was acquired from Sigma-Aldrich, Germany.

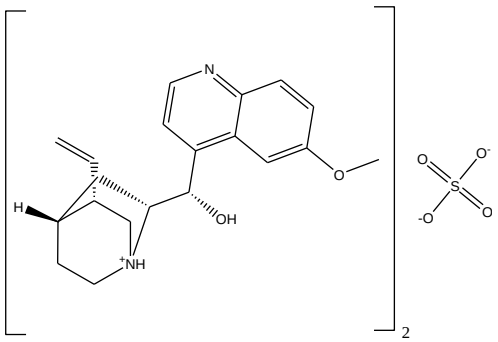

Figure 4A.2: Structure of quinine sulfate

4A.2.2. Characterization

Characterization of structural features of carbon dot was done by the same FTIR and NMR instruments as reported in the previous chapters. The elemental composition of carbon dot was determined by energy dispersive X-ray spectroscopic study (EDX, JSM-6390LV). The amorphous nature and the interlayer spacing of carbon dot were measured by same X-ray Diffractometer as described in sub-chapter 3A. The morphology, microstructure and selected-area electron diffraction (SAED) pattern of carbon dot were analyzed by same high resolution transmission electron microscope, HR-TEM as mentioned in sub-chapter 3A. UV-visible absorption spectrum of carbon dot in aqueous solution was recorded using UV spectrometer, Hitachi (U2001, Tokyo, Japan). The photoluminescence (PL) spectra were recorded using a photoluminescent setup (Perkinelemer, Singapore PTE Ltd., Singapore, Model LS 55) in aqueous solution. The quantum yield of carbon dot was determined at excitation wavelength of 360 nm by the following equation,

$$Q_{CD} = Q_R \cdot \frac{I_{CD}}{I_R} \cdot \frac{A_R}{A_{CD}} \cdot \frac{\eta_{CD}^2}{\eta_R^2} \quad \text{..... (4A.1)}$$

where ‘Q’ is the quantum yield, ‘I’ is the intensity of luminescent spectra, ‘A’ is the absorbance at exited wavelength and ‘η’ is the refractive index of used solvent; using quinine sulfate (quantum yield 54) in 0.1 M H_2SO_4 solution as the reference. The subscripts ‘CD’ for carbon dot and ‘R’ for reference are used in this equation.

4A.2.3. Synthesis of carbon dot from banana juice

Carbon dot was synthesized by simply heating of banana juice in a glass bottle. In a typical procedure, a banana (ca. 80 g) was cut into small pieces and pasted with 100 mL of water. Then, 20 mL of the juice (pulp-free, solid content 52 mg/mL) was taken with 20 mL of ethanol in a 60 mL glass bottle, plugged with cotton cork and heated at constant temperature

of 150 °C in an oven for 3.5-4 h. The dark brown product was obtained after cooling at room temperature. This was dissolved in 20 mL of water and the residue was separated by filtration. 50 mL of ethanol was added into the aqueous filtrate and centrifuged at 960×g (5000 rpm) for 15 min under ambient conditions to separate the large particles. The solvent was evaporated at room temperature under vacuum to obtain highly fluorescent carbon dot. The yield of the desired carbon dot was 600 mg (58% mass yield).

4A.3. Results and discussion

4A.3.1. Synthesis and characterization of carbon dot

Carbon dot was synthesized by carbonization of banana juice which contains carbohydrates like glucose, fructose, sucrose and ascorbic acid as the carbon precursors. Although literature reported the possible schematic route for the formation of carbon dot obtained by hydrothermal method from carbon precursor,[24] but there is no clear and details mechanism for the same. Thus, a detail possible mechanism is proposed for the formation of carbon dot from banana juice as shown in **Scheme 4A.1**, based on the literature reports of carbonization of carbohydrates.[30-32] At first hydrolysis, dehydration and decomposition of different carbohydrates were taken placed in the presence of ascorbic acid and resulted soluble compounds like furfural aldehydes, ketones and several organic acids like acetic, levulinic, formic, etc., which acted as acid resources for different acid catalytic reactions (**Scheme 4A.1**). Polymerization and condensation of these products transformed them to different soluble polymeric products. The aromatization and carbonization were then taken placed via condensation and cyclo-addition reactions (**Scheme 4A.1**). Finally, carbon dot was obtained by a probable nuclear burst of these aromatic clusters at a critical concentration of supersaturation point. Here, the presence of ascorbic acid in banana promoted the reaction at low temperature to occur within a short time. All the intermediates suggested by the mechanism are found in the literature.[30-32]

The formation of carbon dot with an average size of 3 nm was confirmed from TEM micrographs as shown in **Figure 4A.3**. TEM image clearly reveals that the synthesized carbon dot particles are spherical in shape with a narrow size distribution ranging between 1.5 to 4.5 nm (**Figure 4A.3b**). These finer particles with narrow distribution are plausible due to the use of milder conditions compared to literature reports. The elemental compositions as the weight and atomic ratios of C and O of carbon dot estimated from EDX data (**Figure 4A.4a**) were 63.39:35.69 and 70.07:29.61 respectively. A minor amount (0.92% in weight or 0.31% in atomic ratio) of potassium was also found due to the use of banana resource, which

contains this element. The different oxygenous functional groups and linkages in carbon dot were evident by FTIR data (**Figure 4A.4c**). In this spectrum, stretching frequency at 3492, 2935, 1730, 1625, 1422, 1264 and 918 cm^{-1} indicated the presence of O-H, C-H, C=O, C=C, C-O-C, C-O and epoxy ring respectively.[24] The presence of these functional groups imparts excellent water solubility of the synthesized carbon dot. The NMR spectra (**Figure 4A.5**) revealed the presence of four different kinds of chemical environment in around the four different regions as discussed below. In ^{1}H NMR spectrum (**Figure 4A.5a**), the regions are found at 1-3 ppm (for sp^3 C-H protons), 3-6 ppm (for the protons attached with hydroxyl, ether and carbonyl groups), 6-8 ppm (for the aromatic or sp^2 protons) and 8-10 ppm (for the aldehydic protons).[12] Also in ^{13}C NMR spectrum (**Figure 4A.5b**), similar four regions viz. 20-80 ppm (for sp^3 carbons and carbons attached with hydroxyl groups), 80-100 ppm (for carbons attached ether linkages), 100-120 ppm (for C=C aromatic or sp^2 carbons) and 175-190 ppm (for C=O carbons) are found.[12] XRD pattern (**Figure 4A.4b**) of carbon dot showed a broad peak at 21.1° corresponds to the (002) peak of graphitic carbon atoms.[13] This indicated the interlayer spacing (d) of carbon dot (0.42 nm) is higher than that of the graphitic interlayer spacing (0.33 nm) along with greater broadening. This confirmed the poor crystalline nature of carbon dot, which is attributed to the generation of more oxygen containing groups. This is further confirmed by SAED pattern of carbon dot as shown in **Figure 4A.3d**.

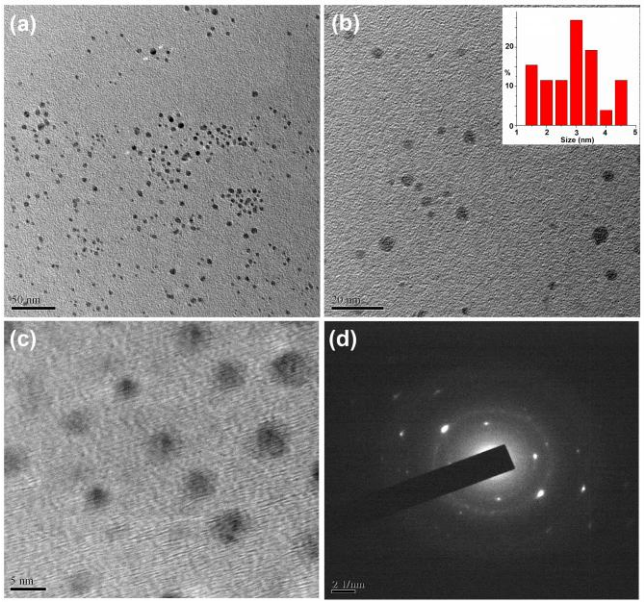

Figure 4A.3: TEM micrographs at different magnifications (a) 50 nm (b) 20 nm (with size distribution, inset) and (c) 5 nm, and (d) SAED pattern of carbon dot

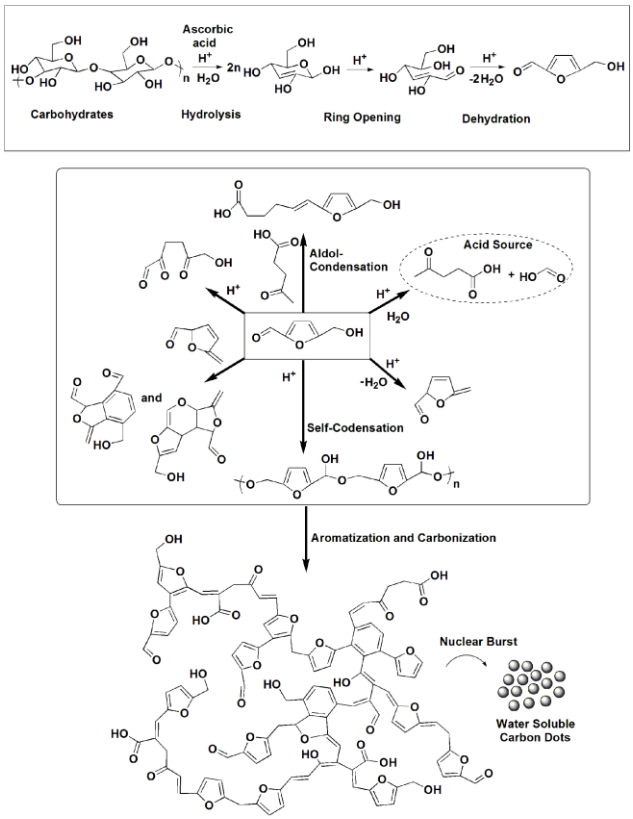

Scheme 4A.1: Possible mechanism for the formation of carbon dot particles

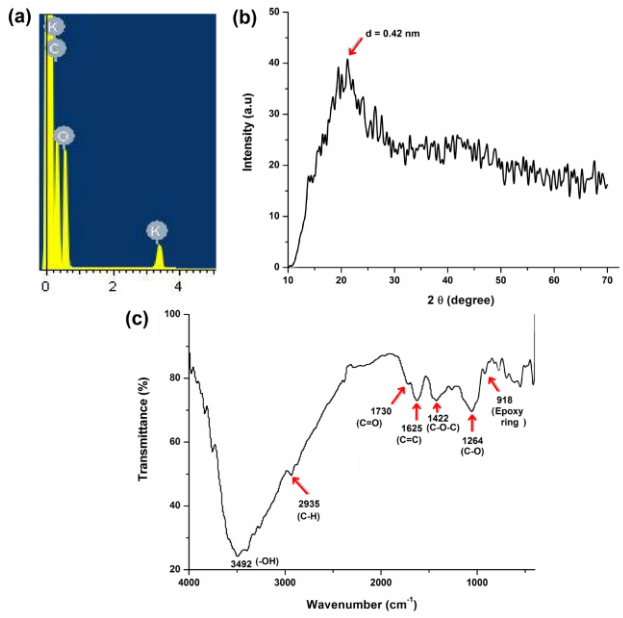

Figure 4A.4: (a) EDX spectrum, (b) XRD pattern and (c) FTIR spectrum of carbon dot

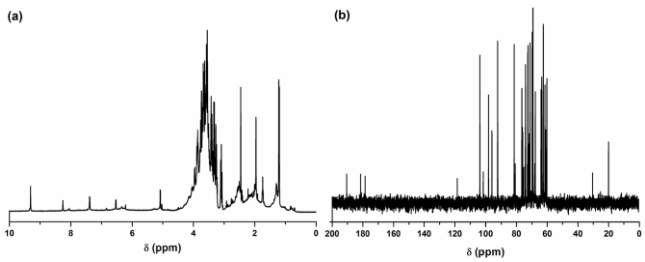

Figure 4A.5: (a) ^{1}H NMR and (b) ^{13}C NMR spectra of carbon dot

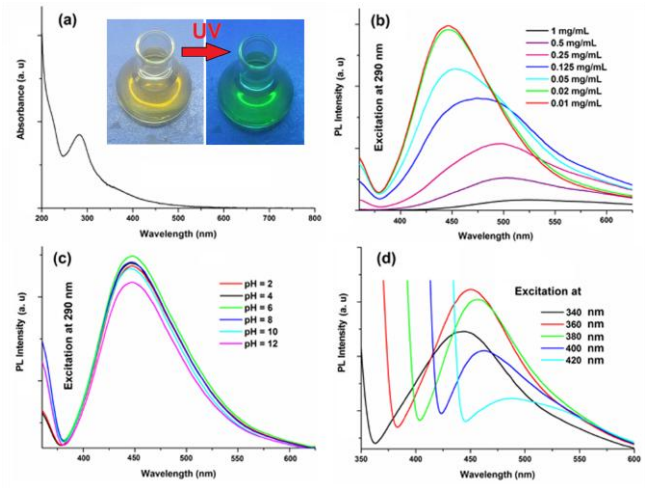

Figure 4A.6: Spectra of carbon dot for (a) UV absorption, and PL with variation of (b) concentration, (c) pH and (d) excitation wavelength (340-420 nm)

4A.3.2. Property of carbon dot

The optical absorption peak of carbon dot was observed at UV region with maximum absorption at 283 nm and a tail extending in the visible range (**Figure 4A.6a**). This is attributed to the n-π* transition of the C=O band and π-π* transition of the conjugated C=C band.

The classic signature of carbon dot is emission wavelength and size dependent PL behavior. From the fundamental as well as application viewpoint, PL is one of the most fascinating behaviors of carbon dot. The synthesized carbon dot in aqueous solution shows green luminescence on exposure of UV light as shown in the inset of **Figure 4A.6a**. From PL spectra of carbon dot (**Figure 4A.6b**), it was cleared that the PL intensity is dependent on the concentration of carbon dot. The intensity of PL spectra sharply increased with the decrease of carbon dot concentration. This may be due to the decreasing interactions among the different polar groups at low concentration. The presence of high amount of polar functionalities helps to form agglomeration at high concentration. PL intensity was also

dependent on excitation wavelength. PL spectra of carbon dot with the variation of excitation wavelength (340-420 nm) are shown in **Figure 4A.6d**. A strong PL emission peak located at 460 nm was observed while excited at 360 nm. The emission peak was also shifted to the higher wavelength with the increase of the excitation wavelength and hence shown clearly in **Figure 4A.7**. The mechanism of PL behavior of carbon dot is very complicated and has not yet been clearly reported. The plausible reasons of PL behavior are the presence of different particle size and the distribution of the different surface energy traps of carbon dot.[13,24] The difference in position of emission peak is due to the variation in size of carbon dot. The energy gap increases with the decrease of size of carbon dot and vice-versa due to the quantum confinement effect like semiconductor quantum dots. Thus, the particles with lower size are got excited at lower wavelength, whereas higher size are got excited at higher wavelength. The intensity of the PL depends on the number of particles excited at a particular wavelength. The highest PL intensity of carbon dot was observed on excitation at 360 nm wavelength due to the highest number of particles were excited in that wavelength. Another reason of the excitation dependent PL behavior of carbon dot is the nature of surface. The presence of various functional groups on the surface of carbon dot may result in a series of emissive traps between π and π^* of C=C. On illuminating carbon dot at a certain excitation wavelength a surface energy trap dominates the emission. As the excitation wavelength changes other corresponding surface state emissive traps become dominant. Hence, the PL mechanism is controlled by both the size effect and the surface defect. In **Figure 4A.6c**, the variation of PL intensity with pH (2-12) is shown. The strong PL intensity was observed at pH range of 4-8. This is due to the electronic transitions of π-π^* and n-π^* that are changed by refilling or depleting their valance bands with the variation of pH.[12] Quantum yield of carbon dot in aqueous solution was found to be 8.95 according to Equation 4A.1 using quinine sulfate (reference) and intensity of PL spectra shown in **Figure 4A.8** as obtained on excitation at 360 nm wavelength. This value is higher than the literature reported values for non-passvating carbon dot. Thus, the PL characteristic of the prepared carbon dot is promising for its different possible applications.

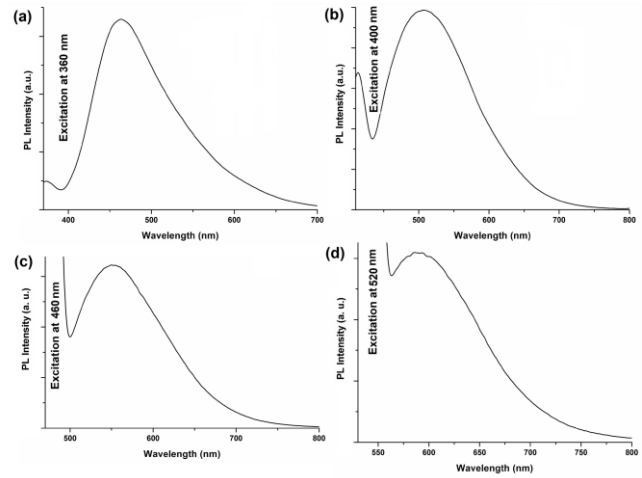

Figure 4A.7: PL emission spectra of carbon dot at (a) 360 nm, (b) 400 nm, (c) 460 nm and (d) 520 nm excitation wavelengths

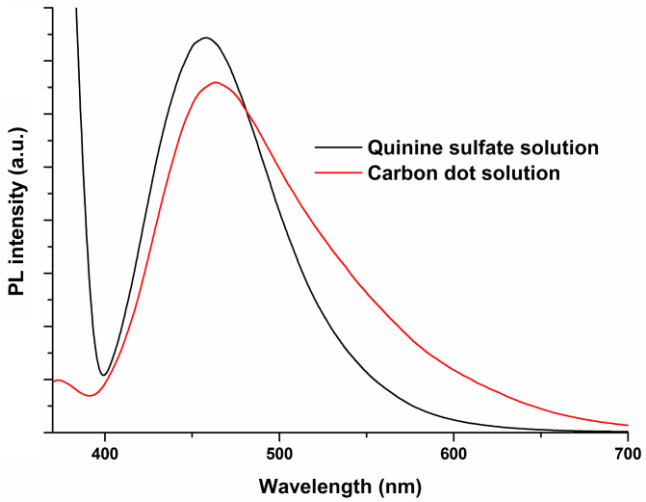

Figure 4A.8: PL spectra of quinine sulfate and carbon dot solution on excitation at 360 nm wavelength

4A.4. Conclusion

So, from this study, we have demonstrated a facile, simple and mass scale synthesis of a water soluble green fluorescent carbon dot from a cheap and readily available natural resource. It exhibited concentration, pH and excitation wavelength dependent interesting photoluminescence behavior at visible range with high quantum yield. So, this bio-based and water soluble high luminescent carbon dot might be potentially applied in solution state optoelectronics.

4B. *Ex-situ* prepared hyperbranched epoxy/carbon dot nanocomposites

4B.1. Introduction

Development of epoxy/quantum dot nanocomposites is demonstrated to improve the performance of hyperbranched epoxy as well as to achieve high transparency and high luminescence solid films for advanced optoelectronic applications as mentioned in the introduction of sub-chapter 4A. Further, recent literature reports support the utilization of carbon dot in light emitting polymer nanocomposites for different optoelectronics including light emitting device (LED). Zhou et al. synthesized polysaccharide based amphibious fluorescent carbon dot and it was incorporated in poly(methyl methacrylate) and poly(vinyl alcohol) matrices to obtain light emitting polymer nanocomposites.[33] Hao et al. incorporated carbon dot into poly(ethylene glycol) to produce poly(ethylene glycol)/carbon dot nanocomposite film with tunable blue-red light emission.[34] A freestanding luminescent film from poly(methyl methacrylate) and nitrogen-rich carbon dot was fabricated by Kwon et al. for white light emitting device.[35] However, the performance including mechanical properties of the nanocomposites was not reported in these investigations. Further, attributes of high mechanical properties, high thermal stability, excellent adhesive strength, good weather and chemical resistance, high transparency and others endow a unique position to epoxy thermosets in the domain of optoelectronics compared to the other polymers as stated in Chapter 1. Thus, in the present sub-chapter carbon dot based hyperbranched epoxy nanocomposites were fabricated by using the conventional technique. As discussed in the previous sub-chapter that carbon dot contains large number of polar oxygenating functionalities, so these can help to disperse it in any polar solvents as well as in the polar polymer matrix like epoxy resin. Thus, solution technique is chosen for the fabrication of hyperbranched epoxy nanocomposites. The presence of carbonized aromatic structure in carbon dot combined with highly polar surface functional groups can lead to good physicochemical interactions with the hyperbranched epoxy and the hardener. This may offer simultaneous improvement in strength and toughness. Further, the unison of quantum size and good compatibility of carbon dot with the matrix may also result in transparent thermosets, unlike what can be achieved with other carbon based nanomaterials like graphene or CNT. In addition, the optical emission in different UV regions of carbon dot of different sizes in the epoxy matrix may lead to useful materials for optical devices like light-emitting diodes and UV light detector systems as well as in anti-counterfeiting applications.

Thus, in the present study, luminescent transparent hyperbranched epoxy nanocomposites with outstanding toughness and elasticity were created by incorporation of very little amount of carbon dot (≤1 wt%).

4B.2. Experimental

4B.2.1. Materials

TAHE20 was used as the matrix in this study like previous chapter. Thus, the materials and processes were used in this study related to TAHE20 resin and thermoset are same as described in sub-chapter 2B. The same carbon dot as reported in sub-chapter 4A was used for the fabrication of nanocomposites.

4B.2.2. Characterization

The characterization and instrumentation methods for spectroscopic, microscopic, XRD and mechanical testing were same as reported in sub-chapter 2B and 4A. Here, the percentages of transmittance of the nanocomposites films were calculated from UV-visible absorption spectra. The visual transparency of the nanocomposites was checked by a pen mark covered with the thin thermosetting films (thickness of 0.3-0.4 mm). The optical color emission photos of the nanocomposite films, logos, and fingerprint were recorded in a UV light chamber (Test Master, Kolkata, India). The dilute ethanolic solution of the nanocomposite was used to make a fingerprint on a white paper and dried at 60 °C for 1 h. The PL spectra of nanocomposites films (0.3-0.4 mm) were recorded using same PL instrument as described in previous sub-chapter.

4B.2.3. Preparation of nanocomposites

The hyperbranched epoxy/carbon dot nanocomposites were prepared by *ex-situ* solution technique. The requisite amount (0.1, 0.5, and 1.0 wt % solid carbon dot) of an ethanolic solution of carbon dot was added to the bulk hyperbranched epoxy polymer, and the mixture was stirred mechanically for 4 h followed by ultrasonication for 10 min at room temperature using same ultrasonic processor as described in sub-chapter 3A, section 3A.2.3.2. Then, 50 wt% of poly(amido-amine) (PAA) hardener was added to the mixture, and the components were mixed homogeneously at room temperature. The mixture was coated on glass plates (75 × 25 × 1.3 mm^3) for the scratch hardness and tensile test and on steel plates (150 × 50 × 1.6 mm^3) for the impact resistance test. The plates were cured at 100 °C for a specified time after being degassed under vacuum for 24 h at room temperature. Then, the cured thin films

(thickness of 0.3-0.4 mm) were peeled off from the glass plates by immersing in hot water (70 °C), and the films were dried under vacuum at room temperature. The nanocomposites were named ECD0.1, ECD0.5, and ECD1.0, corresponding to 0.1, 0.5, and 1.0 wt% of carbon dot, respectively.

4B.3. Results and discussion

4B.3.1. Preparation and characterization of the nanocomposites

The nanocomposites of hyperbranched epoxy and carbon dot were prepared by *ex-situ* solution technique with the help of mechanical shearing and ultrasonication forces. Carbon dot was added only in 0.1, 0.5 and 1.0 wt% with respect to the amount of epoxy resin. The curing time of the nanocomposites with PAA at 100 °C decreases with the increase of amount of carbon dot (**Table 4B.1**). This is due to the presence of a large numbers of polar functional groups (like hydroxy, epoxy, carbonyl, ether, etc. as revealed from FTIR spectrum) in carbon dot which took part in the crosslinking reaction (**Scheme 4B.1**). This also resulted in a strong interfacial interaction with the hyperbranched epoxy matrix. In the FTIR spectrum (**Figure 4B.1a**), for the hyperbranched epoxy, following characteristic absorption bands were observed (ν_{max}/cm^{-1}): 3391 (-OH), 2963 (C-H), 1606 (C=C), 1241 (C-O), 1037 (C-C) and 914 (oxirane),[36,37] whereas the bands for carbon dot were found at (ν_{max}/cm^{-1}): 3492 (-OH), 2935 (C-H), 1730 (C=O), 1625 (C=C), 1422 (C-O-C), 1264 (C-O) and 915 (oxirane) as described in sub-chapter 4A.[24] In the FTIR spectrum of the nanocomposite, a broad band for -OH stretching frequency was observed at 3290 cm^{-1}. This shift compared to pristine polymer is due to the strong interactions and chemical crosslinking of carbon dot with the hyperbranched epoxy and PAA hardener. The carbonyl peak of carbon dot (1730 cm^{-1}) was also shifted to 1670 cm^{-1} after the formation of nanocomposites. This is because of the formation of amide linkages by the reaction of carboxylic acid and ester groups of carbon dot with the amino groups of the hardener. The oxirane bands of the hyperbranched epoxy polymer (914 cm^{-1}) and carbon dot (915 cm^{-1}) completely vanished in the nanocomposite due to their participations in chemical crosslinking reaction. The formation of nanocomposites further diminished the crystallinity of the poorly crystalline carbon dot as the intensity of the peak of carbon dot at 21° in XRD (**Figure 4B.1b**) was found to be decreased. The peak was also broadened and shifted to 18° in the nanocomposites. This is due to the disordered arrangement of the atoms caused by the strong interactions of the polar functional groups of carbon dot and the polymer matrix. The poor crystallinity of carbon dot, which was further decreased by the formation of nanocomposites, is also confirmed by the selected area electron

diffraction (SAED) pattern of carbon dot (**Figure 4A.3d**, sub-chapter 4A) and ECD0.5 (**Figure 4B.2c**). An excellent dispersion of carbon dot in the polymer matrix was supported by TEM micrograph (**Figure 4B.2a**) of ECD0.5. The fine dispersion of carbon dot is due to the chemical binding to the polymer matrix through their large number of functional surface groups during the curing reaction, which is preventing agglomeration. The internal spacing of carbon dot was increased after the formation of nanocomposites as shown in the inset picture of the TEM image. A tendency for aggregations of carbon dot in the hyperbranched epoxy matrix was observed in the TEM image (**Figure 4B.2b**) for ECD1.0. Here we speculate that at higher carbon dot concentration the large number of polar functional surface groups may also favor interactions of the nanodot particles. Further, it is assumed that at this concentration all functional groups are not participated in chemical reaction with the polymer matrix.

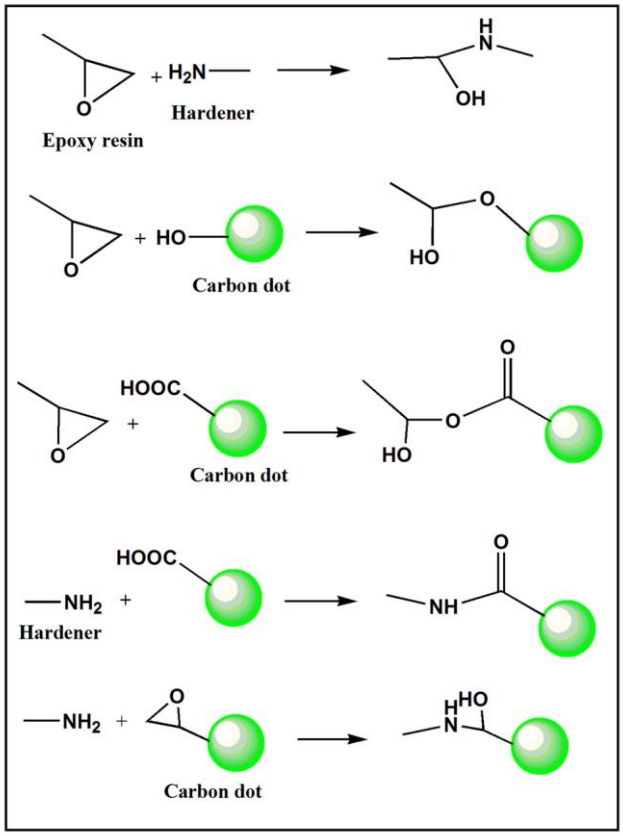

Scheme 4B.1: Crosslinking reactions among the hyperbranched epoxy, PAA hardener and carbon dot

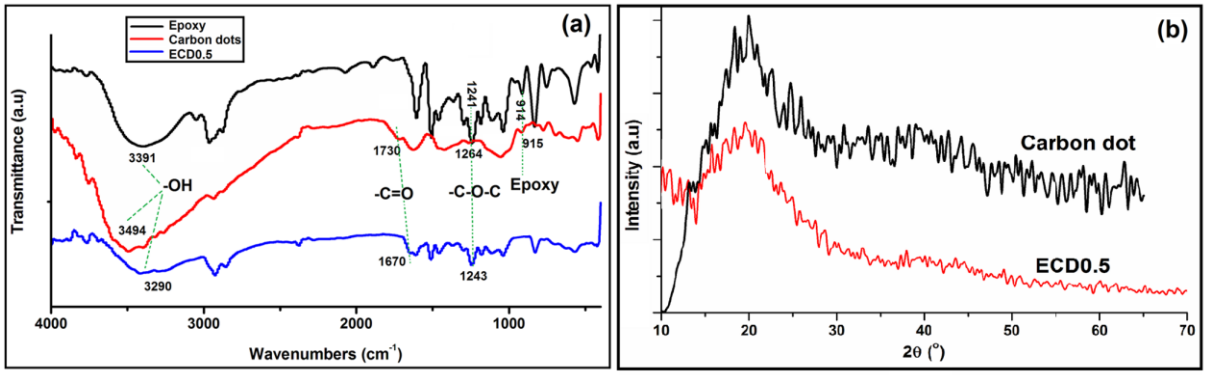

Figure 4B.1: (a) FTIR spectra of hyperbranched epoxy, carbon dot and nanocomposite (ECD0.5); and (b) XRD patterns of carbon dot and nanocomposite (ECD0.5)

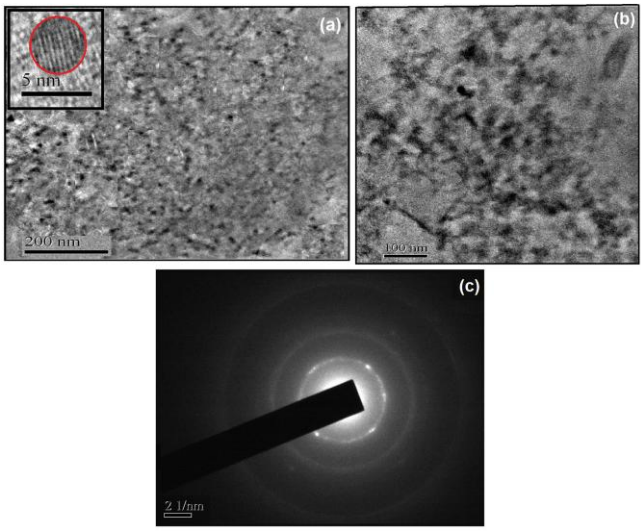

Figure 4B.2: TEM images of (a) ECD0.5, overview picture and individual integrated carbon dot with internal structure (insert in the picture) and (b) ECD1.0; and (c) SAED pattern of ECD0.5

4B.3.2. Mechanical properties of the nanocomposites

Mechanical properties like tensile strength, elongation at break, toughness, impact resistance, scratch hardness and bending values of the pristine hyperbranched epoxy and the nanocomposites are given in **Table 4B.1**. From the results, it is found that the elongation at break and the toughness of the hyperbranched epoxy thermoset were dramatically enhanced after the formation of nanocomposites even at very low loading (max. 1.0 wt%) of carbon dot. The tensile strength and scratch hardness of the pristine epoxy were also improved by the formation of the nanocomposites. The tensile strength increases with the increase of carbon dot content as evident from the stress-strain profiles (**Figure 4B.3**). However, the tensile

strength of ECD1.0 was lower than ECD0.5. This might be due to the some aggregations of carbon dot in the polymer matrix as shown in the TEM image of ECD1.0 (**Figure 4B.2b**). The nanocomposites also exhibited high impact resistance and flexibility. Since both, the pristine hyperbranched epoxy thermoset as well as the nanocomposites reached the measurement limits of the instruments for impact resistance (100 cm), flexibility evaluation (1 mm), and scratch resistance (10.0 kg), the enhancement of these values by adding carbon dot could not be quantified. But, these results clearly indicate a dramatic enhancement of toughness of the hyperbranched epoxy thermoset by the incorporation of a very low amount of carbon dot. The stress-strain profiles (**Figure 4B.3**) also revealed an up to 350% improvement in elasticity of the epoxy thermoset by the formation of nanocomposites. This simultaneous improvement in strength, toughness and flexibility of the hyperbranched epoxy is a commendable achievement. This is due to the presence of the carbonized aromatic core structure combined with a high number of polar surface functional groups in carbon dot.[38] This provides, on the one hand, a strong and stiff nanomaterial, which is enhancing mechanical properties of the polymer matrix; and on the other hand, a very strong physico-chemical interactions between the nano dot and the matrix, which is further enhanced by the very small size of carbon dot resulting in large surface area. The polar functional groups (like hydroxyl, epoxy, carbonyl, ether, etc.) of carbon dot take part in the physical and chemical crosslinking reactions with the hyperbranched epoxy resin and the hardener as shown in **Scheme 4B.2**. The strong interfacial interaction of carbon dot with the matrix helps to enhance the rigidity, as reflected by the enhancement of strength. All these combined effects enhance the overall performance including tensile strength, elongation at break and toughness of the thermoset.

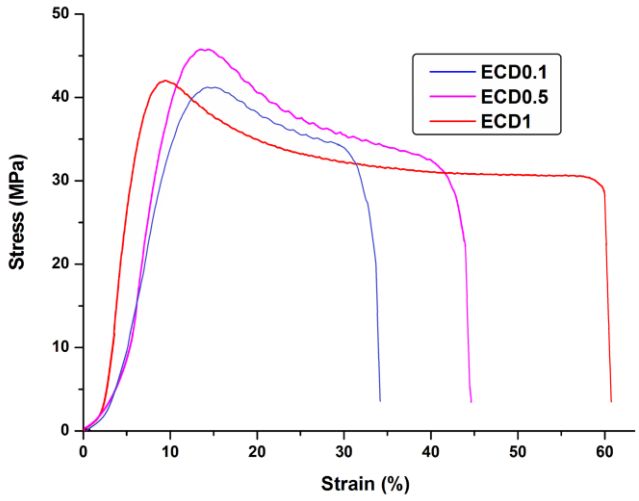

Figure 4B.3: Stress-strain profiles of the nanocomposites

Table 4B.1: Performance of the nanocomposites

Parameter	TAHE20*	ECD0.1	ECD0.5	ECD1.0
Curing at 100 ^{o}C (min)	70 ± 1	60 ± 2	45 ± 1	40 ± 2
Swelling (%) at 25 ^{o}C	23 ± 0.5	21 ± 0.8	20 ± 0.9	20 ± 0.6
Tensile strength (MPa)	40 ± 1.0	40.7 ±1.4	46 ± 1.8	42 ± 1.3
Elongation at break (%)	21 ± 0.8	34 ± 1.6	45 ± 1.3	61 ± 1.2
Toughness (MPa)	570 ± 8	982 ±12	1452 ±18	1889 ±19
Impact strength (cm)	>100	>100	>100	>100
Scratch hardness (kg)	9.0 ± 0.5	>10.0	>10.0	>10.0
Bending dia. (mm)	>1	>1	>1	>1
Adhesive strength, W-W (MPa)	2680 ±12	4691±18	>5678±8	>5686±14
Adhesive strength, M-M (MPa)	2662±9	4272±7	7060±19	9136±26

*As reported in sub-chapter 2B

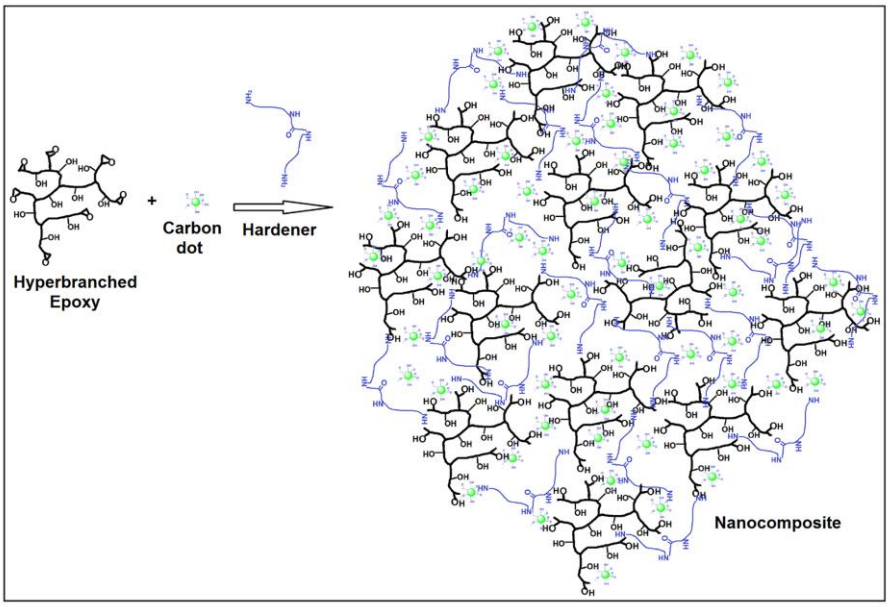

Scheme 4B.2: Different physico-chemical interactions of carbon dot particles with hyperbranched epoxy and PAA hardener

4B.3.3. Adhesive strength of the nanocomposites

Lap-shear tests revealed more than two and three fold enhancement in adhesive strength for wood and metal substrates, respectively, by the incorporation of only 1.0 wt% carbon dot into

the hyperbranched epoxy thermoset (**Table 4B.1**). This is due to the presence of polar functionalities in the nancocomposites allows for strong interactions and physical interlocking with the substrates, and these interactions increase with the increase of the amount of carbon dot in the thermoset.[36] In case of ECD0.5 as well as ECD1.0, substrate failure was observed for wood joint and thus, the nanocomposites exhibited even higher adhesive strength than the reported values (**Table 4B.1**). Different polar functional groups of cellulosic wood substrate strongly interacted with the polar functional groups present in the hyperbranched epoxy, carbon dot and PAA hardener. For the metal substrate, however, strong physical interlocking with hyperbranched epoxy and different functional groups of carbon dot is the main reason for high adhesive strength. The strong physical interlocking is due to the easy diffusion of low viscous hyperbranched epoxy and hardener along with the spherical fine particles of carbon dot into the surface structure of the metal substrate.

4B.3.4. Optical properties of the nanocomposites

Optical properties like transparency and luminescence of carbon dot based polymer nanocomposites are not only interesting but also unique. These characteristics are difficult to achieve from other carbon based nanocomposites. The transparency of the cured hyperbranched epoxy resin is not much affected after formation of nanocomposites with carbon dot as can be seen for ECD0, ECD0.5 and ECD1.0 in **Figure 4B.4a**. The retention of high transparency in the nanocomposites is due to the quantum size (below 10 nm) of carbon dot and the high dispersion quality retaining their nanoscale size in the thermoset due to the chemical crosslinking with the hyperbranched epoxide and the hardener. The percent of transmittance of visible light of the nanocomposite films slightly decreased at low wavelength, as shown in **Figure 4B.4b**, due to absorption of the light source by carbon dot in the low wavelength of visible light as shown in sub-chapter 4A. The optical colors of the nanocomposites in the visible, short UV (254 nm) and long UV (365 nm) region are shown in **Figure 4B.5**. The brown color of the nanocomposite in the visible range was changed into bluish green by illumination with of the short UV light and to dark blue under long UV light. The green and blue color emissions in the nanocomposites are due to the corresponding band gaps of carbon quantum dot at the two excitation wavelengths. The color change at different wavelengths of UV light is due to the presence of different sizes of carbon dot in the nanocomposites as demonstrated in sub-chapter 4A. Carbon dot with lower size get excited at short UV region and carbon dot with higher size are excited at long UV region. The maximum optical absorption of the nanocomposites was observed in the UV region but it is

extending up to the visible range with low intensity (**Figure 4B.6a**). This is due to the n-π* transition of the C=O band and π-π* transition of the conjugated C=C band.[13] The classic signature of carbon dot is a PL behavior, which is the most fascinating property of carbon dot from the application point of view. This PL behavior is due to the quantum size of carbon dot, which results in a large band gap due to the quantum confinement effect. In the PL study of the nanocomposites, a strong emission peak located at 450 nm was observed while excited at 360 nm (**Figure 4B.6b**). The intensity of the PL spectra sharply increased with the increase of carbon dot content. This is due to the fact that the PL intensity depends on the number of particles excited at a particular wavelength as described in sub-chapter 4A. As the number of particles increases with the increase of concentration of carbon dot in the nanocomposites, so ECD1.0 shows the highest PL intensity.

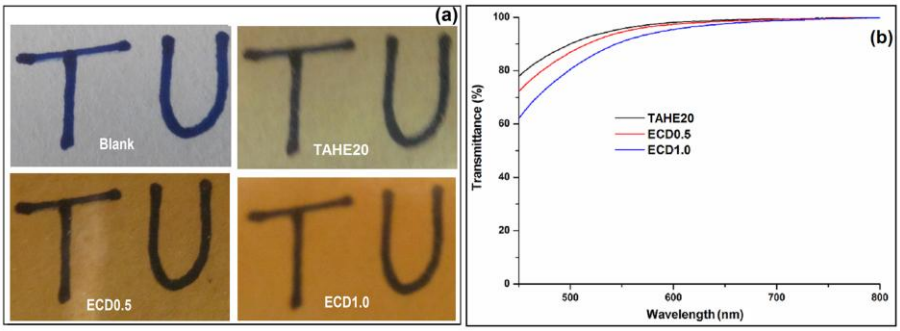

Figure 4B.4: (a) Photos for transparency and (b) visible light transmittance (%) of pristine epoxy and nanocomposite films

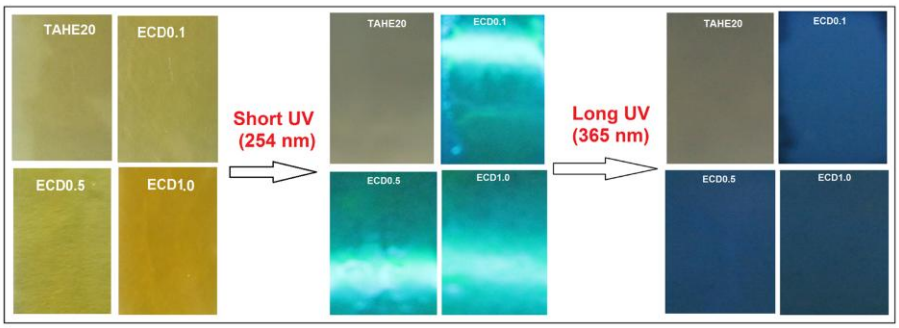

Figure 4B.5: Photos of hyperbranched epoxy thermoset and nanocomposites films at visible, short and long (from left to right) UV regions

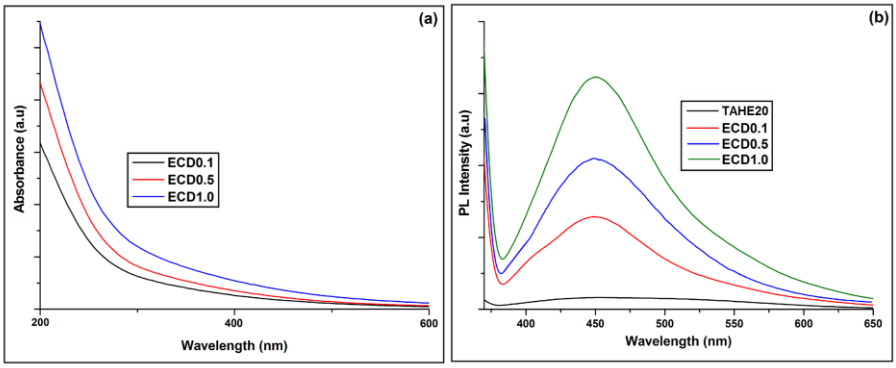

Figure 4B.6: (a) UV and (b) PL spectra of the nanocomposites

4B.3.5. Application for anti-counterfeiting

The prepared nanocomposites are not only useful as a high performance advanced functional material, but it can also be used for multifunctional anti-counterfeiting application. As the nanocomposites were soluble in different solvents or even can form stable emulsion in water before curing, so the dilute solution or an emulsion of the nanocomposites can be used for anti-counterfeiting of different documents or delicate designs including logo and fingerprints.[39] The fingerprint was colorless under visible light but resulted in a fluorescent color under the exposure of UV light of 365 nm (**Figure 4B.7**). It is pertinent to mention here that the same utility can also be achieved by using different inorganic semiconductor quantum dots or organic dyes. But in this case, the presence of large number of polar functional groups both in the matrix and the nanomaterials offers strong interaction with the substrate of interest. Further, the thermoset also provides water proofing characteristic in addition to strengthening the substrate. The study showed that the strength of a cellulosic substrate increased up to three fold after application of this thermoset. Thus, the present studied material has multifold advantages in anti-counterfeiting application.

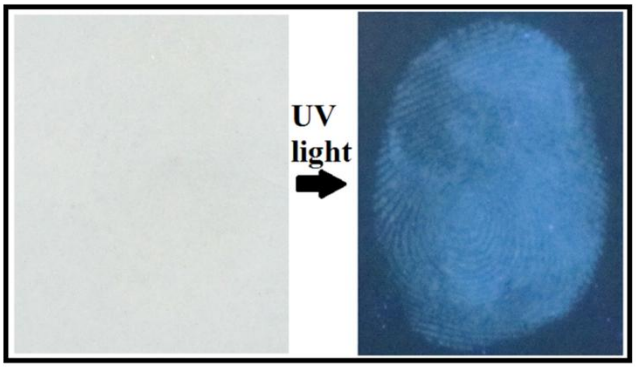

Figure 4B.7. Luminescent photo of fingerprint under UV exposure at 365 nm

4B.4. Conclusion

In summary, we demonstrated an outstanding tough, elastic, transparent and flexible hyperbranched epoxy thermosetting nanocomposite with interesting optical properties by incorporation of a very small amount of carbon dot of ≤1 wt%. This may open up a new avenue for epoxy thermoset as functional nanocomposite film for advanced optical applications. The high adhesive strength of these thermosetting nanocomposites combined with their advanced properties significantly broadens the application range in advanced technologies. This achievement of huge nano effect of carbon dot might be transferred to other polymers. The emission at different UV regions may be useful in optical devices like light emitting diodes and UV light detection system as well as in multifunctional anti-counterfeiting application.

4C. *In-situ* prepared hyperbranched epoxy/carbon dot nanocomposite

4C.1. Introduction

The previous sub-chapter addresses the development of epoxy/quantum dot nanocomposites with adequate performance especially the toughness of the hyperbranched epoxy through the formation of nanocomposite with carbon dot. However, the improvement of the performance including transparency and luminescence properties is not so significant for advanced optoelectronic applications as they are merely physical mixtures of epoxy and carbon dot as like all other reported polymer/carbon dot *ex-situ* nanocomposites.[33-35] In contrary, carbon dot has large number of peripheral polar functional groups such as hydroxyl, carboxylic, epoxy, etc., which can provide an opportunity to be used as a reactive functional nanomaterial for the fabrication of *in-situ* polymer nanocomposite. Literature also support the formation of epoxy *in-situ* nanocomposites with different functionalized nanomaterials like graphene oxide, carbon nanofibers, etc. for effective reinforcement.[40-42] However, in all such reports mainly studies were confined on performance like mechanical properties and rheological behavior of the nanocomposites. The functionalized nanomaterials were also mixed with epoxy monomers before curing them, but not used as reactive component during the synthesis of epoxy resin. Thus, it is an interesting proposition to use carbon dot as one of the reactive components in synthesis of such resin and nanocomposite. Further, such approach also helps in uniform and homogeneous dispersion of carbon dot in the synthesized hyperbranched epoxy matrix, which in turn results strong interfacial interactions between them. It is therefore expected that the resultant nanocomposite will exhibit tremendous improvement in performance including optical property.

In the present sub-chapter, thus a carbon dot based high performance light emitting and transparent hyperbranched epoxy *in-situ* nanocomposite was fabricated where carbon dot used as a reactive component during the preparation of hyperbranched epoxy. The performance of this thermosetting nanocomposite was also compared with the pristine hyperbranched epoxy as well as hyperbranched epoxy/carbon dot nanocomposite obtained through *ex-situ* solution technique.

4C.2. Experimental

4C.2.1. Materials

Pentaerythritol (PE) as the branched generating moiety was used in this study, as it provides high performance and high transparency to epoxy resin. PHE4h was also used for comparison purpose, as it possessed the highest overall performance among the PHE thermosets. The same carbon dot used in the previous two sub-chapters was used in the present work. All other materials like solvents, PAA hardener, etc. used in this sub-chapter were same as used in the sub-chapters 2A, 4A and 4B.

4C.2.2. Characterization

Here also same instrumentation and characterization techniques were used as reported in the previous two sub-chapters. Only the optical color emission photos of the resins and nanocomposite films were recorded in a UV fluorescence inspection cabinet (Labotech Solutions, India).

4C.2.3. Methods

4C.2.3.1. Preparation of hyperbranched epoxy/carbon dot *in-situ* nanocomposite (CHE)

PHE4h/carbon dot *in-situ* nanocomposite (coded as CHE) was prepared by the same procedure as described in sub-chapter 2A for PHE4h resin using the same reactants and same amount under the same conditions. Here, only 1 wt% of carbon dot (with respect to the synthesized PHE4h resin in sub-chapter 2A) was added with the 5 N aqueous solution of NaOH.

4C.2.3.2. Preparation of hyperbranched epoxy/carbon dot *ex-situ* nanocomposite (ECP)

PHE4h/carbon dot *ex-situ* nanocomposite (coded as ECP) was prepared by the solution technique with the help of mechanical shearing and ultrasonication similar to the last sub-chapter for the preparation of hyperbranched epoxy/carbon dot nanocomposites. Here 1 wt% carbon dot was mixed with PHE4h.

4C.2.3.3. Curing of the nanocomposites

CHE and ECP were cured with 50 wt% poly(amido-amine) (PAA) hardener by the same procedure as described for PHE4h in sub-chapter 2A.

4C.3. Results and discussion

4C.3.1. Fabrication and characterization of the nanocomposites

PHE4h resin was synthesized by an $A_2 + B_4$ polycondensation reaction as reported in the sub-chapter 2A. Initially, DGEBA (A_2) was formed in the reaction mixture as reactivity of BPA with ECH is greater than PE as the former contains aromatic proton. Finally, PHE4h resin was formed by the reaction between DGEBA (A_2), PE (B_4) and ECH. On the other hand in case of CHE, carbon dot contains sodium salt of reactive phenolic and carboxylic acid groups as carbon dot was mixed with NaOH solution. The formation of sodium salt increases the reactivity of the phenolic and carboxylic groups by increasing nucleophilicity of the groups. Thus, here DGEBA and ECH were reacted with reactive carbon dot as well as PE to form hyperbranched epoxy *in-situ* nanocomposite as shown in **Scheme 4C.1**. The structural features of PHE4h resin and CHE were characterized by FTIR and NMR studies, which also confirmed the participation of carbon dot in the reaction to form hyperbranched epoxy *in-situ* nanocomposite. In the FTIR spectrum (**Figure 4C.1**) of PHE4h resin, the stretching vibrations are attributed to the following features (ν_{max}/cm^{-1}): 919 and 835 (oxirane), 3457 (O-H), 3055 (aromatic C-H), 2970 (aliphatic C-H), 1606 (aromatic C=C), 1450-1510 (C-O-C), 1244 (C-O) and 1035 (C-C) as reported in sub-chapter 2A.[36,37] In case of carbon dot, the stretching vibrations of FTIR spectrum are (ν_{max}/cm^{-1}): 3492 (-OH), 2935 (C-H), 1730 (C=O), 1625 (aromatic C=C), 1422 (C-O-C), 1264 (C-O) 918 and 780 (oxirane),[24] whereas, in FTIR spectrum of CHE, the stretching vibrations (ν_{max}/cm^{-1}) are attributed to the following features: 919 and 835 (oxirane), 3444 (O-H), 3062 (aromatic C-H), 2971 (aliphatic C-H), 1764 (C=O), 1460-1510 (C-O-C), 1614 (aromatic C=C), 1244 (C-O) and 1037 (C-C). The hydroxyl and carboxylic acid stretching frequencies of carbon dot (at 3492 and 1730 cm^{-1} respectively) are shifted to 3444 and 1764 cm^{-1} in CHE due to their participation in different chemical reactions during the formation of hyperbranched epoxy *in-situ* nanocomposite as shown in **Scheme 4C.1a**. In ^{1}H NMR spectrum (**Figure 4C.2a**) of PHE4h resin, δ_H (400 MHz, $CDCl_3$, Me_4Si, ppm) values indicate the following structural features: 3.3 (1H, oxirane), 2.7 and 2.9 (2H, oxirane), 3.9 (2H, $4CH_2$ of PE), 1.6 (3H, CH_3 of BPA), 6.8 (4H, BPA), 7.1 (4H, BPA), 1.9 (1H, OH), 4.2 (1H, CHOH), 4.0 (2H, CH_2 attached with oxirane), 3.9 (2H, CH_2 attached with oxygen atoms of PE unit) and 4.1 (2H, CH_2 attached with oxygen atoms of BPA unit).[36,37] Whereas, in ^{1}H NMR spectrum (**Figure 4C.2b**) of CHE, the same δ_H (400 MHz, d_6-DMSO, Me_4Si, ppm) values are present along with 5.7-6.2 (aromatic protons of carbon dot), 4.8-5.2 (HC=CH of carbon dot), 3.6 (protons attached with ether of carbon dot) and 1.0-1.4 (sp^3 protons of carbon dot), which are also present in ^{1}H NMR spectrum of pristine carbon dot (**Figure 4C.2c**). The carboxylic acid and phenolic protons of carbon dot in the range of 7.5-9.5 ppm are not present in ^{1}H NMR spectrum of CHE, which confirms that

these functional groups were participated in the reaction during preparation of CHE *in-situ* nanocomposite. In ^{13}C NMR spectrum (**Figure 4C.3a**) of PHE4h resin, the δ_C (d_6-DMSO, ppm) values were observed at 43 (CH_2, oxirane), 49 (CH, oxirane), 46-47 (central C of PE unit), 114, 127, 143 and 156 (4C of BPA), 31 (CH_3, BPA unit), 41 (C, isopropediene of BPA unit), 68 (CH_2, PE unit) and 62-67 (CH_2-O units and CHOH unit).[36,37] All these δ_C (d_6-DMSO, ppm) are present in ^{13}C NMR spectrum (**Figure 4C.3b**) of CHE along with 20-30 (sp^3 carbons of carbon dot), 65-68 (carbon dot carbons attached with ether linkages), 80-100 (sp^2 carbons of carbon dot) and 170-180 (carbonyl carbons of carbon dot), which are also present in ^{13}C NMR spectrum (**Figure 4C.3c**) of carbon dot. The degree of branching (DB) of PHE4h resin was determined from ^{13}C NMR spectrum as reported in the sub-chapter 2A and it was found 0.78. It was calculated from the integration values of the central carbon atom of PE for the four units (two D, one L and one T units) were observed at δ = 46.75, 46.55, 46.40 and 46.20 ppm respectively, as shown in inset picture of **Figure 4C.3a**. However, in case of CHE structural characterization by DB is very difficult as carbon dot also took part in the reaction with *in-situ* formed DGEBA and other reactants as shown in **Scheme 4C.1**. The calculated DB based on the above mentioned peaks was found to be 0.52, excluding the participation of carbon dot.

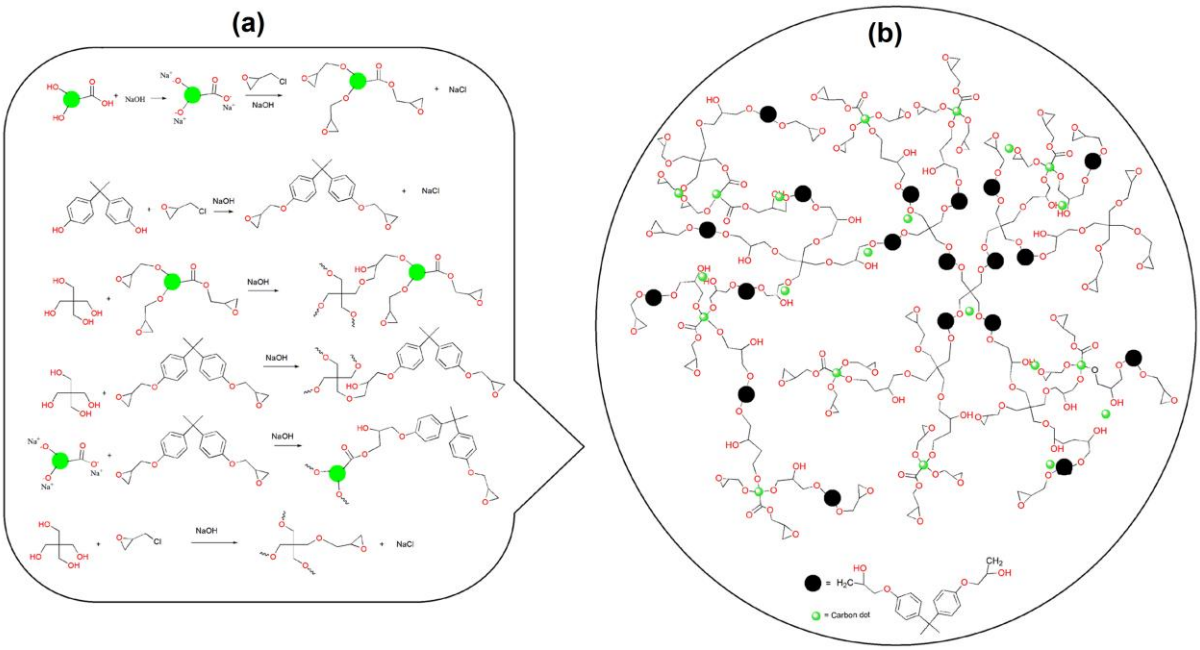

Scheme 4C.1: (a) Chemical reactions of the reactants and carbon dot during the formation of CHE *in-situ* nanocomposite and (b) its general structure

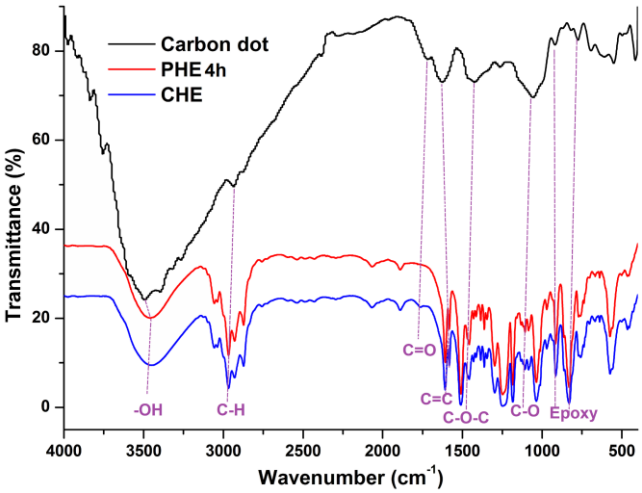

Figure 4C.1: FTIR spectra of carbon dot, PHE4h resin and CHE

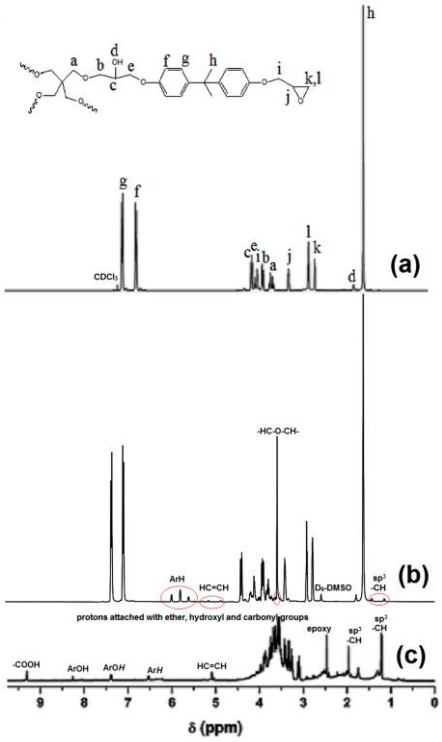

Figure 4C.2: ^{1}H NMR spectra of (a) PHE4h resin, (b) CHE and (c) carbon dot

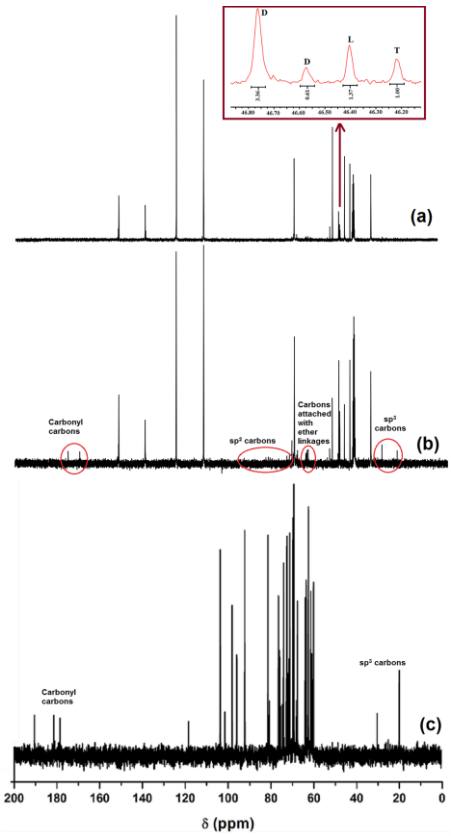

Figure 4C.3: ^{13}C NMR spectra of (a) PHE4h resin, (b) CHE and (c) carbon dot

The epoxy equivalent, hydroxyl and viscosity values of PHE4h resin and CHE are given in **Table 4C.1**. The numbers of epoxy as well as hydroxyl groups of the hyperbranched epoxy are higher for CHE than PHE4h due to participation of carbon dot in the former. As the number of these polar functional groups are higher in CHE compared to PHE4h resin, so the viscosity of the former is also higher (<1.5 folds), due to the presence of more intra- and inter- molecular attraction in CHE. Again, when carbon dot was physically mixed with PHE4h resin (i.e. in case of ECP) the viscosity increased more than four folds as the polar functional groups (hydroxyl, carboxylic acid, epoxy, ether, etc. as revealed from FTIR spectrum) of carbon dot are totally free to interact (by different physical interactions including polar-polar) with polar functional groups of PHE4h resin. The inner structure of CHE and ECP were examined by HR-TEM analysis. The uniform and homogenous dispersion of carbon dot inside CHE was observed in **Figure 4C.4a**. This uniform dispersion is due to the chemical bond formation of the functional groups of carbon dot during the preparation of *in-situ* nanocomposite. However, in case of ECP, a few amounts of carbon dot particles are agglomerated inside PHE4h matrix due to the intra molecular attraction of the polar functional groups of carbon dot as shown in **Figure 4C.4b**. Thus, the interlayer spacing

(d_{001}) of carbon dot is more affected in case of CHE compared to ECP as shown in **Figure 4C.4(c-e)**. The graphitic d_{001} spacing of carbon dot increases from 0.24 to more than 1.0 nm after the formation of CHE, whereas it increases up to 0.33 nm after the formation of ECP. The poor crystalline structure of carbon dot becomes amorphous after the formation of CHE, as shown in SAED patterns in **Figure 4C.5**. The bright spots in SEAD pattern of carbon dot (**Figure 4C.5a**) are completely disappeared from SAED pattern of CHE (**Figure 4C.5c**), whereas few bright spots are found in SAED pattern of ECP (**Figure 4C.5b**). This is due to the fact that after the formation of CHE by the reaction of carbon dot with DGEBA, PE and ECH, the poor crystalline nature of carbon dot changes to completely amorphous.

Table 4C.1: The values of physical parameters for PHE4h, CHE and ECP

Parameter	PHE4h*	CHE	ECP
Epoxy equivalent (g/eq.)	394	360	-
Hydroxyl value (mg KOH/g)	100	144	-
Viscosity (Pas) at 25 °C	2.99	4.36	12.9

*As reported in sub-chapter 2A

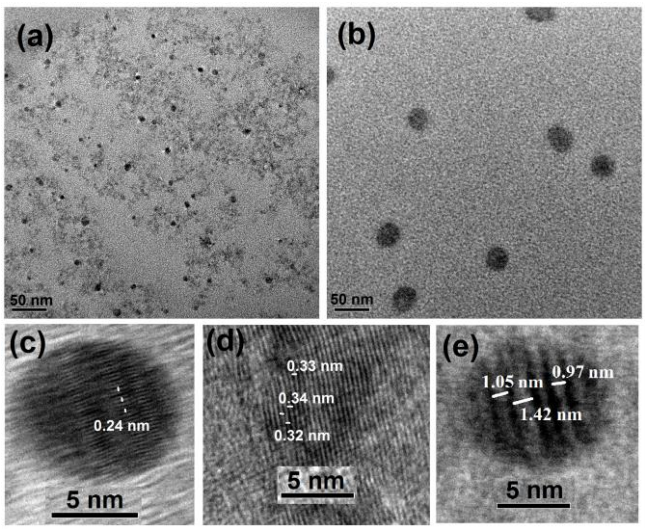

Figure 4C.4: HR-TEM images of (a) CHE and (b) ECP at low magnification, and internal structure of (c) carbon dot, (d) ECP and (e) CHE at very high magnification

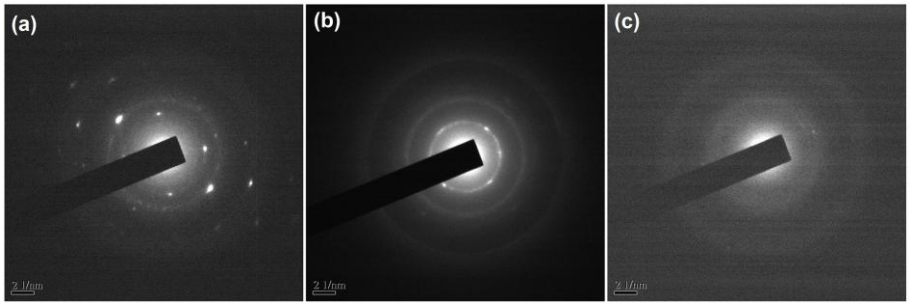

Figure 4C.5: SAED patterns of (a) carbon dot, (b) ECP and (c) CHE

4C.3.2. Curing of the resin and nanocomposites

PHE4h resin, CHE and ECP were cured at 100 °C with 50 phr of PAA hardener for 45 min and the resulted swelling values of the thermosets are given in **Table 4C.2**. PHE4h resin, CHE and ECP took 35, 30 and 45 min curing times respectively to reach <30% swelling value. However, for better comparison all of them cured at same temperature (100 °C) for same time (45 min) with same amount of hardener (50 wt%), though the swelling values were kept in optimum (20-30%).[36] The possible reactions occurred during the curing process were the reactions between amine groups of the hardener with the strained epoxy oxirane rings of PHE4h, CHE and ECP. Again, the hydroxyl, carboxylic acid and epoxy groups of carbon dot (in case of ECP) also took part in the curing reaction, however they took long time due to agglomeration of few amount of carbon dot inside PHE4h matrix. As CHE possesses the highest number of epoxy groups (lowest epoxy equivalent, as given in **Table 4C.1**), so it has the lowest swelling value. However, in case of ECP, as carbon dot was physically mixed with PHE4h, it exhibited the highest swelling value.

Table 4C.2: Performance of PHE4h, CHE and ECP thermosets

Parameter	PHE4h*	CHE	ECP
Swelling value (%)	22±0.2	21±0.5	27±0.8
Tensile strength (MPa)	51±1.0	62.5±2.0	44±1.4
Elongation at break (%)	37±0.5	45±1.3	62±2.5
Toughness (MPa)	1432	1682	2299
Scratch hardness (kg)	>10.0	>10.0	>10.0
Impact resistance (cm)	>100	>100	>100
Bending diameter (mm)	<1	<1	<1
Initial degradation temperature (°C)	279	291	235

*As reported in sub-chapter 2A

4C.3.3. Mechanical properties of the thermosets

Mechanical properties like tensile strength, elongation at break, toughness, scratch hardness, impact resistance and bending values of PHE4h, CHE and ECP thermosets are given in **Table 4C.2**. The stress-strain profiles of the thermosets are shown in **Figure 4C.6**. From these results, it is found that CHE thermoset possessed the highest tensile strength value. This is due to the fact that the carbonized aromatic carbon dot is chemically bonded (covalently bonded) with DGEBA and PE during the formation of hyperbranched epoxy *in-situ* nanocomposite.[38] This helps in strong interfacial interactions and uniform dispersion of carbon dot with compact structural architecture. It also exhibited higher elongation at break compared to PHE4h thermoset. This may be due to the sliding of carbon dot layers at high stress as it is seen from **Figure 4C.4e** that the distance between the layers are increased after the formation of CHE. This increased layer spacing and strong covalent bonds easily overcome the interlayer interactions between carbon dot sheets.[43] As CHE thermoset possessed higher tensile strength and elongation at break, it also showed higher toughness compared to PHE4h thermoset as calculated from the area under stress-strain curves (**Figure 4C.6**). However, tensile strength value of PHE4h thermoset is decreased after physically mixed with carbon dot in ECP thermoset. This is due to the fact that in case of ECP physical interactions of carbon dot with PHE4h are predominated over the chemical bond formation and carbon dot particles are agglomerated inside the PHE4h matrix as observed from the TEM image (**Figure 4C.4b**). Thus, elongation at break and toughness values of PHE4h were increased after the formation of ECP thermoset. PHE4h, CHE and ECP thermosets exhibited the same values of scratch hardness and impact resistance as the values reached the highest limit of the instruments for scratch hardness (10 kg) and impact resistance (100 cm). They also exhibited the lowest limit of the instrument for flexibility evaluation (1 mm bending diameter of mandrel) without any damage to the film.

4C.3.4. Thermal stability of the thermosets

Initial degradation (5 wt% degradation) temperatures (°C) of the thermosets are given in **Table 4C.2**. From the results, it was found that CHE thermoset exhibited the highest thermal stability as carbon dot chemically bonded with the structure of hyperbranched epoxy, which restricted the molecular motion of the polymer chains.[43] Whereas, in case of physical mixture of carbon dot with PHE4h, the thermal stability of the thermoset was decreased as only physical interactions are present in ECP thermoset. However, maximum degradation of the thermosets was started after 300 °C and 50 wt% degradation of them was occurred at ~390

°C as observed from TGA thermograms of the thermosets (**Figure 4C.7**). The thermosets were also degraded by two step patterns, where the first step (~300 °C) is due to the degradation of aliphatic moieties and the second step (~410 °C) is due to the degradation of aromatic moieties.

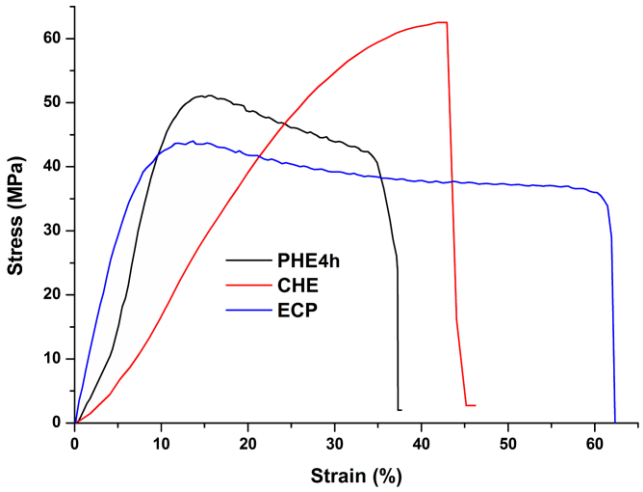

Figure 4C.6: Stress-strain profiles of PHE4h, CHE and ECP thermosets

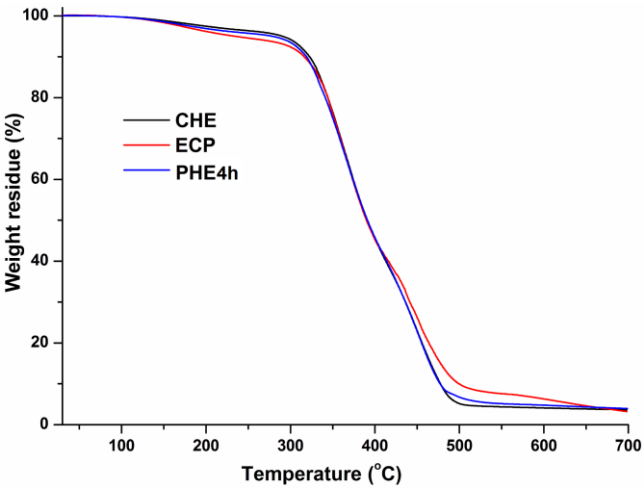

Figure 4C.7: TGA thermograms of CHE, ECP and PHE4h thermosets

4C.3.5. Optical properties

The optical absorbance spectra of PHE4h, CHE and ECP thermosets are shown in **Figure 4C.8a**. The figure shows that the thermosets absorbed more amount light in the UV region. In case of PHE thermoset, absorption of UV light is due to the π-π* transition of aromatic BPA moiety present in its structure. Whereas, in case of CHE and ECP thermosets absorption is due to the π-π* and n-π* transitions of carbon dot as well as the π-π* transition of aromatic

BPA moiety, as reported in the last sub-chapter as well as in literature.[13] From **Figure 4C.8a** it is found that ECP thermoset absorbed the highest amount of UV light because of the presence of only physical interactions between carbon dot and PHE4h, and thus carbon dot particles are free to interact with UV light. However, in case of CHE depletion of the electronic transition was occurred due to the participation of the functional groups of carbon dot in chemical reactions to form hyperbranched epoxy *in-situ* nanocomposite, and thus it absorbed less amount of UV light.

The visual transparency and percent of transmittance of visible light of PHE4h, CHE and ECP thermoset films are shown in **Figure 4C.8b**. In the inset picture, it is found that CHE thermoset film showed the highest transparency. This is due to the quantum size carbon particles with large number of polar functional groups participate in the reaction to form the hyperbranched epoxy nanocomposite. Thus, the percent of transmittance of visible light was also the highest in case of CHE. However, the transparency as well as the percent of transmittance of visible light of PHE4h was decreased after the formation of ECP thermoset. This is due to the presence of only physical interactions between carbon dot and PHE4h as well as agglomeration of carbon dot in the PHE4h matrix.

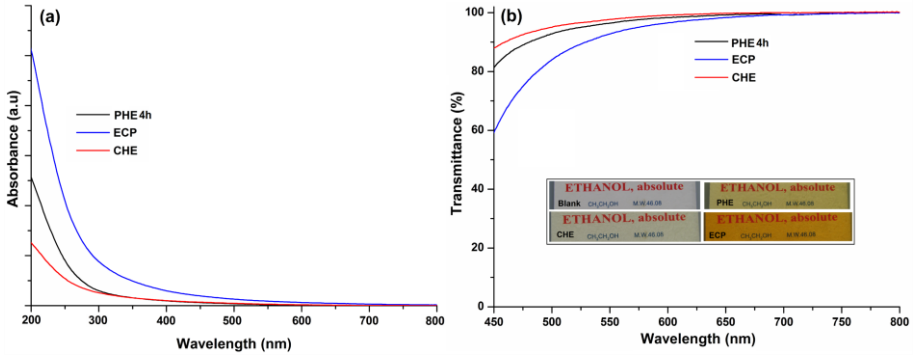

Figure 4C.8: (a) Optical absorbance spectra; and (b) percent of transmittance and transparency (inset pictures) of PHE4h, ECP and CHE thermosets

The PL behaviors of CHE and its thermoset are shown in **Figure 4C.9**. CHE exhibited higher PL intensity as well as spectrum is also narrower compared to carbon dot at the same concentration in ethanolic solution (0.001%) as shown in **Figure 4C.9a**. This is due to uniform dispersion of carbon dot without agglomeration after the formation of CHE. However, after the formation of ECP these were not happened due to the presence of agglomerated carbon dot inside the PHE4h matrix. From **Figure 4C.9b**, it was found that the intensity of the PL spectra increases with the increase of concentration of CHE in ethanolic

solution. On the other hand, in case of carbon dot reverse trend was found, as shown in **Figure 4A.6b** in sub-chapter 4A, because of agglomeration of free carbon dot at higher concentration due to interactions among the polar functional groups on the surface. Whereas, these groups are chemically bonded with other reactants during the formation of CHE, and thus in this case homogeneous and uniform dispersion of carbon dot was observed without any agglomeration. However, CHE also exhibited excitation wavelength dependent PL behavior like carbon dot, as shown in **Figure 4C.9c**. Here, also the highest intensity of PL spectrum was found at 360 nm excitation wavelength which is similar to carbon dot, as reported in sub-chapter 4A. This is common PL behavior of carbon dot and the reason for this behavior is the presence of different particle sizes and the distribution of the different surface energy traps of carbon dot, as reported in sub-chapter 4A as well as in literature reports.[13,24] Quantum yield of CHE was found 12.69 using quinine sulfate as the reference according to Equation 4A.1 in sub-chapter 4A, as measured from PL spectra in **Figure 4C.10** on excitation at 360 nm wavelength, which was higher compared to carbon dot (8.95). This is because of the uniform and homogenous dispersion of carbon dot inside the matrix in CHE compared to bare carbon dot. PL spectra of CHE, ECP and PHE4h thermoset films are shown in **Figure 4C.9d**. From the spectra it was found that CHE thermoset exhibited the highest PL intensity due to strong interfacial interaction of carbon dot with hyperbranched polymer as well as homogeneous and uniform dispersion of carbon dot inside the matrix as stated above. However, PL intensity of PHE4h was not significantly improved after the formation of ECP thermoset as only physical interactions are present and agglomeration of carbon dot was also formed inside the PHE4h matrix. PHE4h thermoset possessed negligible PL due to the presence of aromatic BPA moiety in its structure.

The optical color emissions of carbon dot, CHE as well as CHE and ECP thermosets at different wavelengths of UV light are shown in **Figure 4C.11**. From **Figure 4C.11(a-c)** it was found that CHE as well as CHE thermoset emits green and light blue fluorescence similar to carbon dot after illumination with short (254 nm) and long (365 nm) wavelengths of UV light respectively. The green and blue color emissions are due to the corresponding band gaps of carbon dot at different excitation wavelengths of UV light and the color change is due to the presence of different sizes of carbon dot as reported in the last sub-chapter. ECP thermoset also emits similar color like CHE thermoset (**Figure 4C.11c**), however due to some agglomeration of carbon dot inside the PHE4h matrix brightness of color is inferior to CHE.

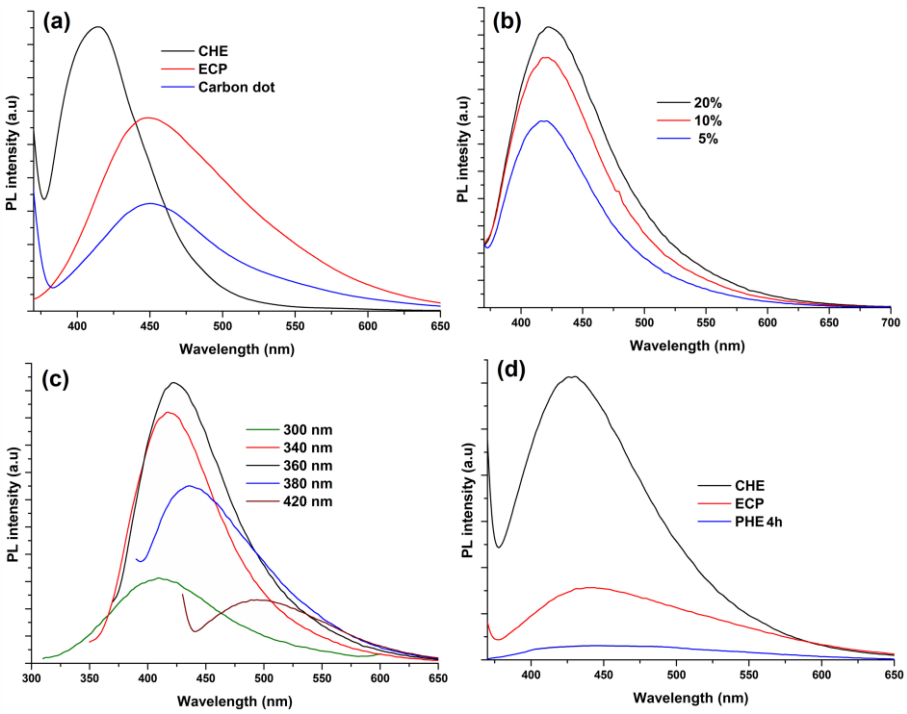

Figure 4C.9: PL spectra of (a) CHE, ECP and carbon dot in ethanolic solution at same concentration (0.001%); (b) CHE (in ethanolic solution) with variation of concentration and (c) variation of excitation wavelength; and (d) CHE, ECP and PHE4h thermosets

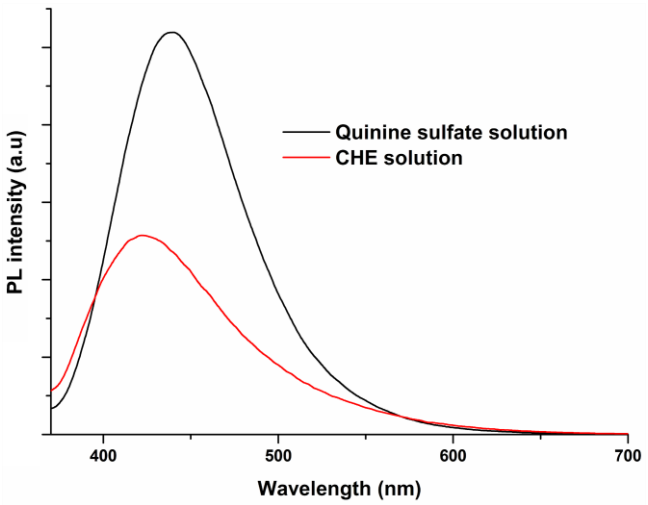

Figure 4C.10: PL spectra of quinine sulfate and CHE solution on excitation at 360 nm wavelength

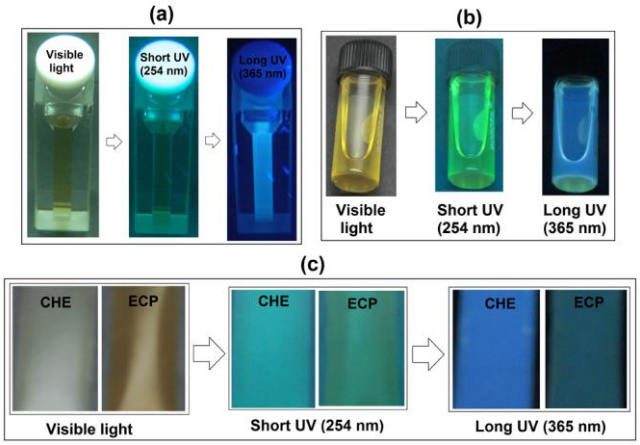

Figure 4C.11: Optical color emissions of (a) carbon dot, (b) CHE; and (c) CHE and ECP thermosets under exposure of UV lights at 254 and 365 nm

4C.4. Conclusion

The present study, therefore, demonstrated an excitation wavelength dependent photoluminescence carbon dot/hyperbranched epoxy *in-situ* nanocomposite. NMR and TEM studies confirmed the participation of carbon dot in chemical reaction during the formation of hyperbranched epoxy *in-situ* nanocomposite. The study also revealed superior mechanical, thermal and optical properties of this nanocomposite over the *ex-situ* nanocomposite of carbon dot with hyperbranched epoxy. These results clearly evident the incorporation of carbon dot in the hyperbranched structure through covalent linkages. Thus, the study may open up a new avenue for high performance transparent fluorescent polymeric materials used in advanced optical applications.

References

1. Kotsilkova, R. *Thermoset nanocomposites for engineering applications*, Smithers Rapra Technology Limited, UK, 2007.
2. Gong, L., et al. Optimizing the reinforcement of polymer-based nanocomposites by graphene, *ACS Nano* **6** (3), 2080--2095, 2012.
3. Liu, T., et al. Preparation and characterization of epoxy nanocomposites containing surface-modified graphene oxide, *J. Appl. Polym. Sci*. **131**, 40236 (6 p), 2014.
4. Zou, W., et al. A transparent and luminescent epoxy nanocomposite containing CdSe QDs with amido group-functionalized ligands, *J. Mater. Chem*. **21**, 13276--13282, 2011.

5. Yang, Y., et al. Transparent and light-emitting epoxy nanocomposites containing ZnO quantum dots as encapsulating materials for solid state lighting, *J. Phys. Chem. C* **112**, 10553--10558, 2008.
6. Li, Q., et al. Photoluminescent carbon dots as biocompatible nanoprobes for targeting cancer cells in vitro, *J. Phys. Chem. C* **114**, 12062--12068, 2010.
7. Goh, E. J., et al. Bioimaging of hyaluronic acid derivatives using nanosized carbon dots, *Biomacromolecules* **13**, 2554--2561, 2012.
8. Yang, S. T., et al. Carbon dots for optical imaging in vivo, *J. Am. Chem. Soc*. **131**, 11308--11309, 2009.
9. Baker, S. N. & Baker, G. A. Luminescent carbon nanodots: emergent nanolights, *Angew. Chem. Int. Ed*. **49**, 6726--6744, 2010.
10. Qiao, Z. A., et al. Commercially activated carbon as the source for producing multicolor photoluminescent carbon dots by chemical oxidation, *Chem. Commun*. **46**, 8812--8814, 2010.
11. Xu, X., et al. Electrophoretic analysis and purification of fluorescent single-walled carbon nanotube fragments, *J. Am. Chem. Soc*. **126**, 12736--12737, 2004.
12. Jia, X., et al. One-pot green synthesis of optically pH-sensitive carbon dots with upconversion luminescence, *Nanoscale* **4**, 5572--5575, 2012.
13. Li, H., et al. Carbon nanodots: synthesis, properties and applications, *J. Mater. Chem*. **22**, 24230--24253, 2012.
14. Sun, Y. P., et al. Quantum-sized carbon dots for bright and colorful photoluminescence, *J. Am. Chem. Soc*. **128**, 7756--7757, 2006.
15. Liu, H., et al. Fluorescent carbon nanoparticles derived from candle soot, *Angew. Chem. Int. Ed*. **46**, 6473-6475, 2007.
16. Qiao, Z. A., et al. Commercially activated carbon as the source for producing multicolor photoluminescent carbon dots by chemical oxidation, *Chem. Commun*. **46**, 8812--8814, 2010.
17. Zhang, J., et al. Controlled synthesis of green and blue luminescent carbon nanoparticles with high yields by the carbonization of sucrose, *New J. Chem*. **34**, 591--593, 2010.
18. Puvvada, N., et al. Synthesis of biocompatible multicolor luminescent carbon dots for bioimaging applications, *Sci. Technol. Adv. Mater*. **13**, 045008, 2012.
19. Zhai, X., et al. Highly luminescent carbon nanodots by microwave-assisted pyrolysis, *Chem. Commun*. **48**, 7955--7957, 2012.

20. Yang, Z. C., et al. Intrinsically fluorescent carbon dots with tunable emission derived from hydrothermal treatment of glucose in the presence of monopotassium phosphate, *Chem. Commun*. **47**, 11615--11617, 2011.
21. Hsu, P. C. & Chang, H. T. Synthesis of high-quality carbon nanodots from hydrophilic compounds: role of functional groups, *Chem. Commun*. **48**, 3984--3986, 2012.
22. Yang, Y., et al. One-step synthesis of amino-functionalized fluorescent carbon nanoparticles by hydrothermal carbonization of chitosan, *Chem. Commun*. **48**, 380--382, 2012.
23. Zhang, Z., et al. Protein as the source for synthesizing fluorescent carbon dots by a one-pot hydrothermal route, *RSC Adv*. **2**, 8599--8601, 2012.
24. Sahu, S., et al. Simple one-step synthesis of highly luminescent carbon dots from orange juice: application as excellent bio-imaging agents, *Chem. Commun*. **48**, 8835--8837, 2012.
25. Du, W., et al. Green synthesis of fluorescent carbon quantum dots and carbon spheres from pericarp, *Sci. Chin. Chem*. 2015, DOI: 10.1007/s11426-014-5256-y.
26. Kung, M. L., et al. Bifunctional peppermint oil nanoparticles for antibacterial activity and fluorescence imaging, *ACS Sustainable Chem. Eng*. **2**, 1769--1775, 2014.
27. Han, S., et al. Fabrication, gradient extraction and surface polarity-dependent photoluminescence of cow milk-derived carbon dots, *RSC Adv*. **4**, 58084--58089, 2014.
28. Park, S. Y., et al. Photoluminescent green carbon nanodots from food-waste-derived sources: large-scale synthesis, properties, and biomedical applications, *ACS Appl. Mater. Interfaces* **6**, 3365--3370, 2014.
29. Wu, Z. L., et al. One-pot hydrothermal synthesis of highly luminescent nitrogen-doped amphoteric carbon dots for bioimaging from *Bombyx mori silk*-natural proteins, *J. Mater. Chem. B* **1,** 2868--2873, 2013.
30. Titirici, M. M., et al. Hydrothermal carbon from biomass: a comparison of the local structure from poly- to monosaccharides and pentoses/hexoses, *Green Chem*. **10**, 1204--1212, 2008.
31. Falco, C., et al. Morphological and structural differences between glucose, cellulose and lignocellulosic biomass derived hydrothermal carbons, *Green Chem*. **13**, 3273--3281, 2011.
32. Ryu, J., et al. Hydrothermal preparation of carbon microspheres from monosaccharides and phenolic compounds, *Carbon* **48**, 1990--1998, 2010.

33. Zhou, L., et al. Amphibious fluorescent carbon dots: one-step green synthesis and application for light-emitting polymer nanocomposites, *Chem. Commun*. **49**, 8078--8080, 2013.
34. Hao, Y., et al. Poly(ethylene glycol)/carbon quantum dot composite solid films exhibiting intense and tunable blue-red emission, *Appl. Surf. Sci*. **311**, 490--497, 2014.
35. Kwon, W., et al. Freestanding luminescent films of nitrogen-rich carbon nanodots toward large-scale phosphor-based white-light-emitting devices, *Chem. Mater*. **25**, 1893--1899, 2013.
36. Barua, S., et al. Glycerol based tough hyperbranched epoxy: Synthesis, statistical optimization and property evaluation, *Chem. Eng. Sci.* **95**, 138--147, 2013.
37. Pavia, D. L., Lampman, G. M., Kriz, G. S. & Vyvyan, J. R. *Spectroscopy*, Cengage Learning India Private Limited, New Delhi, 2007.
38. Konwar, A., et al. Green chitosan-carbon dot nanocomposite hydrogel film with superior properties, *Carbohyd. Polym*. **115**, 238--245, 2015.
39. Liu, Y., et al. Designing lanthanide-doped nanocrystals with both up- and down-conversion luminescence for anti-counterfeiting, *Nanoscale* **3**, 4804--4810, 2011.
40. Bao, C., et al. *In-situ* preparation of functionalized graphene oxide/epoxy nanocomposites with effective reinforcements, *J. Mater. Chem*. **21**, 13290--13298, 2011.
41. Zhu, J., et al. *In situ* stabilized carbon nanofiber (CNF) reinforced epoxy nanocomposites, *J. Mater. Chem*. **20**, 4937--4948, 2010.
42. Zhu, J., et al. Rheological behaviors and electrical conductivity of epoxy resin nanocomposites suspended with *in-situ* stabilized carbon nanofibers, *Polymer* **51**, 2643--2651, 2010.
43. Thakur, S. & Karak, N. Ultratough, ductile, castor oil-based, hyperbranched, polyurethane nanocomposite using functionalized reduced graphene oxide, *ACS Sustainable Chem. Eng.* **2**, 1195--1202, 2014.